Denosumab Alleviates Intervertebral Disc Degeneration Adjacent to a Lumbar Fusion by Inhibiting Endplate Osteochondral Remodeling and Vertebral Osteoporosis in Ovariectomized Rats

Qi Sun
Hebei Medical University
Fa-Ming Tian
North China University of Science and Technology
Fang Liu
North China University of Science and Technology
Jia-Kang Fang
North China University of Science and Technology
Yun-Peng Hu
North China University of Science and Technology
Qiang-Qiang Lian
North China University of Science and Technology
Zhuang Zhou
The Third Hospital of Hebei Medical University
Liu Zhang (zhliu130@sohhu.com)
Hebei Medical University

Research article

Keywords: Osteoporosis, Ovariectomy, vertebral, Endplate, Osteochondral remodeling

Posted Date: July 14th, 2020

DOI: https://doi.org/10.21203/rs.3.rs-41067/v1

Version of Record: A version of this preprint was published at Arthritis Research & Therapy on May 28th, 2021. See the published version at https://doi.org/10.1186/s13075-021-02525-8.

Abstract

Background: Although adjacent segmental intervertebral disc degeneration (ASDD) is one of the most common complications after lumbar fusion, its exact mechanism remains unclear. As an antibody to RANKL, denosumab (Dmab) effectively reduces bone resorption and stimulates bone formation, which can increase bone mineral density (BMD) and improve osteoporosis. However, it has not been confirmed whether Dmab has a reversing or retarding effect on ASDD.

Methods: Three-month-old female Sprague-Dawley rats that underwent L4–L5 posterolateral lumbar fusion (PLF) with spinous-process wire fixation four weeks after OVX surgery were given Dmab four weeks after PLF surgery (OVX+PLF+Dmab group). In addition, the following control groups were defined: Sham, OVX, PLF, and OVX+PLF (n=12 each).Then, manual palpation and X-ray were used to evaluate the state of lumbar fusion. The bone microstructure in the lumbar vertebra and endplate as well as the disc height index (DHI) of the L5/6 were evaluated by microcomputed tomography (μCT). The characteristic alterations of ASDD were identified via Safranin-O green staining staining. Osteoclasts were detected using tartrate-resistant acid phosphatase (TRAP) staining and the biomechanical properties of vertebra were evaluated. Aggrecan (Agg), metalloproteinase-13 (MMP-13), a disintegrin and metalloproteinase with thrombospondin motifs 4 (ADAMTS-4) expression in the intervertebral disc were detected by immunohistochemistry and real-time polymerase chain reaction (RT-PCR) analysis.

Results: Manual palpation showed clear evidence of the fused segment's immobility. Compared to the OVX+PLF group, more new bone formation was observed by X-ray examination in the OVX+PLF+Dmab group. Dmab significantly alleviated ASDD by retaining disc height index (DHI), decreasing porosity of endplate, and increasing the biomechanical properties and BMD of vertebra. TRAP staining results showed a significantly decreased number after Dmab treatment, especially in subchondral bone and cartilaginous endplate. Moreover, the results of protein and mRNA expression in intervertebral disc (IVD) showed that Dmab not only inhibited matrix degradation by decreasing MMP-13 and ADAMTS-4 but also promoted matrix synthesis by increasing Agg.

Conclusions: These results suggest that Dmab may be a novel therapeutic target for the treatment of ASDD.

Introduction

Lumbar fusion is a widely used, principal operation for spinal diseases that effectively relieves the symptoms of lower back pain[1]. Adjacent intervertebral disc degeneration (ASDD), one of the important and prevalent complications of lumbar fusion, seriously affects long-term clinical outcomes for patients[2], requires secondary operations, and increases the costs[1]. The clinical treatment of ASDD is limited because it cannot fully relieve the symptoms induced by degeneration of the intervertebral disc, and it cannot fundamentally reverse ASDD. Therefore, it is necessary to develop new effective therapeutic strategies to ameliorate the progression of ASDD.

Although the etiology of ASDD is complex and insufficiently understood, there is accumulating evidence that endplate osteochondral remodeling and vertebral osteoporosis might play critical roles in ASDD[3]. IVD is composed of the central nucleus pulposus(NP), surrounded by the collagenous annulus fibrosus (AF) and two endplates (EP) located above and below the nucleus pulposus and annulus fibrosus[4]. Commonly, the gelatinous NP is the main functional composition of IVD, and the cellular changes and degradation of extracellular matrix of the NP tissue are major causes of disc degeneration[5]. Anatomically, the vertebrae and IVD are combined into a bundle to form the spine's motor segment. From a mechanical and biological point of view, they are closely connected and considered to be a functional unit. Therefore, the health of vertebral bone and health of intervertebral discs are closely related [6]. In addition, IVD is the largest avascular tissue in the human body; therefore, a bone marrow channel between the EP and NP and AF is essential for absorbing nutrients and exchanging metabolites in the disc. The cells in the outer annulus of the AF receive nutrition mainly from the circumferential pathway while the nucleus pulposus cells almost completely rely on the nutrition provided by the vertebral capillary bed adjacent to the EP [4, 7–9]. Under cyclic loading, the nutrient supply of IVD and discharge of metabolic waste depend on diffusion and fluid flow, which is mainly affected by endplate penetration [10].

Osteoporosis, which is mainly prevalent in postmenopausal and older populations, is characterized by decreased bone mass and reduced bone mineral density (BMD), accompanied by the destruction of bone microstructure, resulting in increased bone fragility and fracture risk [11]. Recent studies have confirmed that osteoporosis is not only an important risk factor for the complications of vertebral nonunion after spinal fusion but also the main inductor of ASDD [6].

Different from other anti-osteoporosis drugs, denosumab(Damb) is a human monoclonal immunoglobulin G2 (IgG2) antibody that competitively binds to receptor activator of nuclear factor kappa-B ligand (RANKL), preventing the binding of RANKL to its osteoclast-derived receptor (RANK), thereby inhibiting osteoclast-induced bone resorption activity [12]. David W Dempster and colleagues[13] demonstrated that denosumab preserved femoral neck cartilage remodeling while retaining modeling-based bone formation, and BMD increased continuously over time. Recent studies have shown that EP cartilage remodeling and vertebral osteoporosis may be important pathogenetic factors of ASDD.

However, it is still unknown whether Dmab can inhibit the remodeling of adjacent intervertebral disc endplate cartilage in lumbar fusion and whether it can improve the prognosis of osteoporotic lumbar fusion in elderly postmenopausal women. In the present study, an ovariectomized rat model was used to investigate the effect of subcutaneous administration of Dmab on ASDD after lumbar fusion, providing a basis for the clinical treatment of ASDD.

Materials And Methods

Experimental animals

All experimental protocols were approved by the Institutional Animal Care and Use Committee. A total of 60 three-month-old female Sprague-Dawley rats (each weighing 259 ± 18 g) (Vital River Experimental Animal Technical Co., Ltd., Beijing, China) were used for this study. The animals were kept in a ventilated environment with a 12:12 h light–dark cycle at a constant temperature of 21 °C.

Operation procedures, groups, and study design

After anesthesia, each rat underwent either sham operation (Sham, only a skin incision was made and then sutured) or bilateral ovariectomy (OVX). Four weeks after OVX surgery, an experimental model of posterolateral spinal fusion (PLF) was established by an intertransverse process fusion using an autologous iliac graft with wire fixation at L4–L5 spinous processes. Finally, the fascia and the skin were closed. The surgical procedure replicated the previously validated model described by Boden and colleagues[14]. All animals were given prophylactic antibiotics (Penicillin-G; 40,000 U) soon after surgery for three days. Then, rats received subcutaneous administration of vehicle or 0.25 mg/mL Dmab five days per week for four weeks in the following groups (n = 12 each): (1) Sham; (2) OVX; (3) PLF; (4) OVX + PLF; and (5) OVX + PLF + Dmab. Weights were recorded weekly, and Dmab doses were adjusted accordingly.

Four weeks after PLF, radiographic evaluation and manual palpation were performed to evaluate the lumbar fusion. Afterward, the L3–L6 segment of the spine was removed, the attached muscles were removed, and the fusion was evaluated manually by palpation. Half of the samples (n = 6,each group) were used for histological and immunohistochemical (L5–L6) and RT-PCR analysis (L3–L4). The other half (n = 6,each group) underwent microcomputed tomography (μCT) scanning and testing of the mechanical properties of the vertebral body.

Evaluation of posterolateral lumbar fusion

After 4 weeks of PLF, the animals were anesthetized and the fusion was evaluated with a soft radiograph(DR7500 System, Kodak, US) in the anteroposterior plane and analyzed by an experienced radiologist blinded to the study,which according to the criteria established by O'Loughlin et al[14]. The animals were killed 8 weeks after the X-ray examination, then, the manual palpation of the fusion site (L4–L5 segment) were performed to assess the fusion status as described by Abe and colleagues[15], which is considered to be a gold standard for detecting pseudoarticulation formation or stabilization of the fixation[16]. Each fusion site was evaluated by three independent observers in a blinded fashion.

μCT analysis

The L5–L6 segment was scanned using a SkyScan 1176 microcomputed tomography system in accordance with a previously described protocol[6]. Briefly, the scanner was operated at a voltage of

80 kV, a current of 313 μA, and a resolution of 18 μm. Images were reconstructed using NRecon v1.6 software, respectively. Three-dimensional (3D) reconstruction images were obtained using CTvox v3.0. The regions of interest (ROI) of vertebrae, endplates, and Disc height index (DHI) were chosen using CTAn v1.14 and DataViewer v.1.5.

After excluding the cortical bone, the transverse images of L6 vertebrae were used to measure the vertebral body. The IVD and vertebral bone heights were measured between L5 and L6 at the mid-sagittal plane, and the DHI was calculated using the following equation(DHI = (Disc height from anterior + Disc height from posterior) / (Vertebral bone height from anterior + Vertebral bone height from posterior))[17]. The ROI of the cartilage endplate was restricted to the visible bone plate that covers the vertebrae. 3D structural parameters of vertebrae included bone volume fraction (BV/TV), trabecular thickness (Tb.Th), trabecular number (Tb.N), and trabecular separation (Tb.Sp). The parameters of the endplate included bone mineral density (BMD), number of closed pores (Po.N(cl); representing the number of pores with a closed cavity in the endplate structure), open porosity (Po(op)); open pore volume over total pore volume), and total volume of pore space (Po.V(tot)).

Compression experiment of vertebral body

Before the beginning of the experiment, all vertebral appendages, including transverse processes, superior and inferior articular processes, pedicles and lamina were removed, and only vertebral body was retained. The upper and lower parts of the vertebral body were polished and standardized to a height of about 5 mm and perpendicular to the longitudinal axis of the vertebral body. It was assumed that the vertebral body was cylindrical, and the average diameter and body boundary area of the standard parts were calculated based on the anterior and posterior diameter of each vertebral body. The lower end of the vertebral body was fixed on the test platform with glue, and the vertebral body was axially compressed at a speed of 4 mm/min until fracture. The maximum compression load and energy absorption values were recorded, and the maximum stress was calculated as the ratio of maximum pressure and body interface area (maximum compressive strength of the vertebral body). During the experiment, normal saline was used to keep the vertebral specimens in a moist state.

Histology and immunohistochemistry examinations

After fixation in 10% neutral paraformaldehyde for 48 h, the L5–L6 segments of the lumbar spine (including the intervertebral disc) were decalcified in 10% EDTA-2Na for three months at room temperature. The decalcified samples were dehydrated and embedded in paraffin. They were subsequently cut into 8-μm-thick sections to perform safranin O and fast green staining, tartrate-resistant acid phosphatase (TRAP) staining, and immunohistochemistry. The images were captured by a microscope system (BX53; Olympus, Tokyo, Japan). The degenerative changes in the L5–L6 segment were assessed using the disc degeneration assessment scoring system described by Koichi Masuda and colleagues[18].

Safranin-O green staining was performed in accordance with the instructions of the reagent kits (Servicebio Biological Technology Co. Ltd., China). TRAP staining was handled according to the protocol of the staining kit (Solarbio Science & Technology Co. Ltd., China).

To observe the tissue expression of aggrecan (Agg), metalloproteinase-13 (MMP-13), a disintegrin and metalloproteinase with thrombospondin motifs 4 (ADAMTS-4), 8-μm-thick sections were deparaffinized, rehydrated, and immunostained. Briefly, after antigen retrieval and inactivation of endogenous peroxidase, the sections were incubated overnight at 4 °C with primary antibodies: Agg (1:500 dilution; Cat. No. GTX54920; GeneTex Inc. USA), MMP-13 (1:200 dilution; Cat. No. GTX55707; GeneTex Inc., USA), ADAMTS-4 (1:200 dilution; Cat. No. ab185722; Abcam Inc., USA). The next day, the sections were incubated with a biotinylated secondary antibody and a streptavidin-biotin complex peroxidase solution. Diaminobenzidine (DAB) chromogen was applied, and the sections were counterstained with hematoxylin.

All images were captured by a BX53 microscope system (Olympus, Tokyo, Japan). The integrated optical density (IOD) values of each factor were semiquantitatively analyzed using Imaging Pro Plus 6.0 software (Media Cybernetics, Rockville, MD, USA). the intensity of positive staining in the ROI was calculated and defined as the sum of integrated optical density (IOD), and the area of ROI was also calculated. The average IOD of specific proteins, reported as IOD/mm^2, was defined as the sum of IOD divided by area of ROI. The final result used for the statistical analysis was the average of values calculated by two individuals who scored the sections in a blinded manner.

RT-PCR

The samples of nucleus pulposus from the L3–L4 intervertebral disc were obtained for this analysis. A Gene Amp 7,700 Sequence Detection System (Applied Biosystems, Foster City, CA) and SYBER® Premix Ex Taq™II kit (Takara, Kusatsu, Japan) were used to perform Reverse transcription (PCR). The primers for genes measured are listed in Table 1. GAPDH was used as an endogenous control. The changes of relative transcript levels of mRNA were reported using the 2 (-Delta Delta C(T)) method as previously described[19]. The experiment was repeated at least three times to ensure accuracy.

Table.1. Sequences of Primers Used for RT-PCR

Gene	Forward Primer (5´-3´)	Reverse Primers (5´-3´)
GAPDH	GGGGAGCCAAAAGGGTCATCATCT	GAGGGGCCATCCACAGTCTTCT
Aggrecan	GAAGTGGCGTCCAAACCAAC	AGCTGGTAATTGCAGGGGAC
ADAMTS-4	CGTTCCGCTCCTGTAACACT	TTGAAGAGGTCGGTTCGGTG
MMP-13	TGCTGCATACGAGCATCCAT	TTCCCCGTGTCCTCAAAGTG

Statistical analysis

All the data were analyzed using SPSS software (SPSS, Chicago, IL, USA), and the results were expressed as means ± SDs. The Shapiro–Wilk test for normality and Bartlett's test for homogeneity of variance were performed. One-way analysis of variance (ANOVA) and Fisher's protected least significant difference test were used to determine the statistically significant differences between the groups. The results of the radiography scores were analyzed using the Kruskal-Wallis test. $P < 0.05$ was considered to be statistically significant.

Results

1.Evaluation of lumbar fusion

To evaluate the fusion of the L4–L5 segment, the segment was examined by X-ray and manual palpation. As shown in Fig. 1, the three groups of animal wires were well fixed. Compared to OVX + PLF, the fusion site of PLF and OVX + PLF + Dmab groups showed a higher radiographic density and more new osteotylus formation. The fusion score of OVX + PLF group was significantly lower than that of PLF and OVX + PLF + Dmab groups($p < 0.05$). OVX + PLF + Dmab group had a lower score than the PLF group, but without reaching statistical significance ($p > 0.05$).

During manual palpation, the wire on the L4–L5 spinous processes of all rats who underwent PLF surgery was well connected to the spinous processes, and there was no detectable movement at the fusion level. These results revealed that the lumbar fusion of rats with PLF was good.

2. μCT parameters of the L5-L6 segments

To quantify vertebral bone and endplate microarchitecture, μCT analysis was performed on L5–L6 segments. Since loss of intervertebral disc height is used as an alternative predictor of intervertebral disc degeneration, the DHI of L5–L6 were measured (Fig. 2A). DHI was significantly lower in the OVX and OVX + PLF groups than in the Sham group($p < 0.05$), while there was no significant difference between OVX and OVX + PLF groups($p > 0.05$). DHI was significantly higher in the OVX + PLF + Dmab group compared to the OVX + PLF group ($p < 0.05$) (Fig. 2B).

As shown in Fig. 3A, compared to the Sham + V group, trabeculae were sparser and the width of the canal between trabeculae was higher in the OVX + V and OVX + PLF groups, and even a large area of bone trabeculae was missing in the OVX + PLF group. The OVX + PLF + Dmab group showed a higher trabecular thickness, lower tube diameter between trabeculae, and more compact trabecular structure compared to the OVX + PLF group. μCT evaluation of L6 vertebra showed that the OVX and OVX + PLF groups had a significantly lower BMD, BV/TV, Tb.Th, and Tb.N, along with higher Tb.Sp, compared to Sham($p < 0.05$). Compared to the OVX + PLF group, there were significantly higher BMD, BV/TV, Tb.Th, and Tb.N, and lower Tb.Sp in the OVX + PLF + Dmab group($p < 0.05$) (Fig. 3B-F).

In addition, a large number of cavities were found in the endplate of the OVX and OVX + PLF groups (Fig. 4A). To determine the degree of porosity in the endplate, μCT parameters of L5–L6 caudal endplate were examined. Compared to the Sham group, the OVX and OVX + PLF groups exhibited significantly lower BMD, BV/TV, and closed pores' number, but significantly higher open porosity and total pore volume($p < 0.05$), all of which reflect higher endplate porosity. However, compared to the OVX + PLF group, the OVX + PLF + Dmab group had a significantly higher BMD, BV/TV, and closed pores' number, as well as lower open porosity and total pore volume($p < 0.05$) (Fig. 4B-E). These results showed that Dmab treatment delayed the reduction of DHI and inhibited vertebral osteoporosis and osteochondral remodeling of the endplate.

3. The evaluation of vertebral mechanical properties

To detect changes in the mechanical properties of adjacent vertebrae, we performed compression tests on L6 segments (Fig. 5A). Maximum load, yield stress, maximum stress, and elastic modulus values were significantly lower in the OVX, PLF, and OVX + PLF groups compared to the Sham group($p < 0.05$). However, Dmab treatment significantly improved the mechanical parameters, compared to the OVX + PLF group($p < 0.05$) (Fig. 5B-E). These data were in accordance with the results of the μCT analysis, verifying the anti-osteoporosis effects of Dmab.

4. The histologic analysis of intervertebral disc between L5-L6 segments

To detect differences in the tissue structure of intervertebral disc among the groups, we performed safranin-O-Fast Green staining. Figure 6 shows that the structure of the intervertebral disc was intact in the sham group. Specifically, many NP cells were accompanied by rich gel-like tissue (extracellular matrix), and AF annulus was arranged regularly and tightly. The boundary between NP and AF was clear. Hyaline cartilage of the endplate contained chondrocytes. In contrast, intervertebral disc degeneration occurred in OVX group, PLF group, and OVX + PLF group to varying degrees. Moreover, the proportion of notochord cells in NP cells was reduced significantly in these groups, and the structural composition of NP was also changed. Some NP cells were replaced by clusters of chondrocyte-like cells, and the matrix around NP cells had varying degrees of mucoid degeneration and uneven distribution. At the same time, the fibrous annulus was broken and disordered. The calcification remodeling in the cartilage endplate increased significantly, the AF annulus was broken and destroyed, and the intervertebral disc was occupied by disorganized fibrochondral tissue. These degenerative changes were the most obvious in the OVX + PLF + V group. Compared to the PLF group, intervertebral disc degeneration was more severe in OVX + PLF group, which confirmed the negative effect of OVX in ASDD. Compared to the OVX + PLF group, pathological changes were effectively controlled in OVX + PLF + Dmab group: the number of notochordal cells in NP was higher, number of chondroid cells was significantly lower, degree of matrix

myxoid degeneration was lower, and AF arrangement of fibers was more orderly. We performed a histological score of the intervertebral disc, which was confirmed by the results($p < 0.05$) (Fig. 7).

5. The turnover and remodeling of vertebral body and endplate cartilage

To discover osteochondral remodeling, TRAP staining was performed. As expected, the results were compatible with the results of μCT and safranin-O-Fast Green staining, suggesting excessive bone and cartilage remodeling because of OVX or PLF. OVX group had a larger number of osteoclasts in cranial and caudal cartilaginous EP compared to Sham, which illustrated the comprehensive effects of OVX on bone and cartilage turnover. However, osteoclasts were observed only in the dorsal part of cartilaginous EP near the lumbar fusion (the spinous process adjacent to L4/5 on the dorsal side of the spine) in the PLF group, where mechanical stress might have been aggregated due to uneven forces caused by lumbar fusion. The combined effects of OVX and PLF resulted in the distribution of a large number of osteoclasts on the trabecular surface of the subchondral bone and cartilaginous EP. After Dmab treatment, the number of osteoclasts was significantly lower($p < 0.05$) (Fig. 8). These results showed that Dmab treatment inhibited turnover and remodeling of vertebral body and endplate cartilage.

6. Composition changes of NP at protein level

Expression of aggrecan, MMP-13, and ADAMTS-4 was detected by immunohistochemistry to assess the matrix metabolism (Fig. 9A-C). In general, gelatinous NP is the main functional composition of IVD, and degeneration of the NP is regarded as a crucial part of intervertebral disc degeneration [20]. Sham group showed the structures of NP with strong immunoreactivity for aggrecan and weak immunoreactivity for MMP-13 and ADAMTS-4. In contrast, the NP showed weak aggrecan immunostaining and strong MMP-13 and ADAMTS-4 immunoreactivity in the OVX, PLF, and OVX + PLF group, especially in the OVX + PLF + V group. However, the OVX + PLF + Dmab group showed stronger immunostaining for aggrecan and weaker immunostaining for ADAMTS-4 compared to the OVX + PLF group($p < 0.05$) (Fig. 9D-F). These results suggested that Dmab may retard the progression of ASDD by changing the content of matrix components in NP.

7. Composition changes of NP at mRNA level

To quantify mRNA expression of aggrecan, MMP-13, and ADAMTS-4 in NPs, the NP tissues of each group were isolated and taken for RT-PCR test. Compared to the Sham group, the OVX + V, PLF + V, and OVX + PLF + V groups showed lower aggrecan and higher MMP-13 and ADAMTS-4 mRNA levels($p < 0.05$). The OVX + PLF + Dmab group showed a higher aggrecan, and lower MMP-13 and ADAMTS-4 mRNA levels compared to the OVX + PLF group□$p < 0.05$□. These results were consistent with immunohistochemical staining (Fig. 10).

Discussion

Considering the high morbidity of ASDD and limitations of current treatment modalities, there is an urgent need to develop a treatment method that delays or even reverses ASDD and preserves the physiological function of the intervertebral disc [21, 22]. Here we demonstrated that Dmab treatment improved the prognosis of lumbar fusion by inhibiting vertebral osteoporosis and endplate cartilage remodeling, also preventing ASDD. These effects of Dmab are beneficial for maintaining the structural and functional integrity of the adjacent vertebral body and endplates, which ensures the patency of the nutritional pathway of the intervertebral disc. In addition, Dmab preserved the normal structure and function of the intervertebral disc by regulating the metabolism of the extracellular matrix in the NP of the IVD.

In further exploration of the pathogenesis of ASDD, we used steel wire to pass through and fix the bases of the spinous processes of L4 and L5. The fragments of the ilium were inserted between the transverse processes of L4 and L5 to simulate spinal fusion in postmenopausal women. X-ray examination showed that the fusion of the L4 and L5 segments was good in PLF, OVX + PLF, and OVX + PLF + Dmab groups, and no activity was detected by manipulation. Microstructural analysis revealed significantly lower DHI in OVX + PLF group than in Sham. The histological score of Safranin-O green staining in OVX + PLF group was significantly higher than that in the Sham group. The immunohistochemical staining and RT-PCR results of nucleus pulposus tissue confirmed that, compared to the Sham group, the expression level of aggrecan was significantly lower whereas the expression levels of ADAMT-4 and MMP-13 were significantly higher in OVX + PLF group. These results are basically consistent with the previous results [2, 3, 23].

In accordance with our previous study, we found a strong correlation between bone mass reduction and intervertebral disc degeneration in ovariectomized rats, which may be related to deterioration of the integrity and function of adjacent structures. Analysis of endplate cartilage remodeling confirmed that microstructure remodeling of subchondral bone caused by osteoporosis may further aggravate osteoarthritis and that the inhibition of subchondral bone remodeling could effectively delay the progression of osteoarthritis. It is suggested that subchondral bone remodeling is an indispensable factor in the development of osteoarthritis. The structures of joints and intervertebral discs are similar [24–26]. To further investigate the relationship of vertebral osteoporosis and subchondral bone remodeling of endplate with ASDD aggravation, we performed μCT analysis of L5–L6 segments in the experimental ASDD model. The results showed obvious focal fragmentation and sparse intersecting bone trabecular areas, as well as varying degrees of calcification of the endplate. The vertebral Tb.Th, Tb.N and BMD decreased significantly, while Tb.Sp increased significantly, suggesting that the subchondral bone structure changed; the endplate BMD and the number of closed pores significantly decreased whereas open porosity and total pore volume increased significantly, suggesting that the subchondral bone microstructure of the endplate was remodeled. It is worth noting that there was severe calcification of the endplates in the OVX, PLF, and OVX + PLF groups, and surprisingly, there was also a certain degree of calcification in the endplates of the Sham group, suggesting that a certain degree of calcification of the endplate cartilage occurs in natural growth conditions.

In addition, after lumbar fusion, vertebral osteoporosis is not only an important risk factor for postoperative vertebral nonunion complications but also leads to increased bone conversion rate and biomechanical changes, resulting in microenvironmental changes, thereby accelerating the development of ASDD [2, 27–29]. We performed TRAP staining on histological sections and found an increased number of osteoclasts, suggesting a high conversion rate of bone and cartilage at the intervertebral disc and vertebral interface in the ASDD model. At the same time, we conducted compression experiments on L6 vertebrae and found that, compared to the Sham group, the ultimate load (maximum load), yield stress, and elastic modulus of L6 vertebrae were significantly lower in OVX and OVX + PLF groups, especially in OVX + PLF group, suggesting a reduced trabecular hardness, increased trabecular brittleness, and altered vertebral biomechanics in ASDD model.

In this study, we used the subcutaneous injection of Dmab. Dmab can effectively block the binding of NF-kB ligand receptor activator (RANKL) to its osteoclast-derived receptor (RANK), thereby inhibiting osteoclast-mediated bone resorption (osteoclast formation, activation, and survival) and promoting bone formation [1, 30]. During a 36-month follow-up, Cummings et al [31] found that Dmab treatment in postmenopausal women could increase vertebral BMD and reduce the risk of vertebral fracture. Here, we showed an improved subchondral bone structure after Dmab treatment compared to the OVX + PLF group (higher BMD, BV/TV, Tb.Th, and Tb.N; lower Tb.Sp of the vertebral body). Manabu Ide et al.[1] confirmed that in addition to increasing BMD, Dmab also effectively improved lumbar fusion. Indeed, we showed that X-ray fusion score of OVX + PLF + Dmab group was significantly higher than that of OVX + PLF group, and there were more new bone formation and higher X-ray optical density at the fusion site of L4–L5, confirming that Dmab could promote bone formation and facilitate the fusion of lumbar vertebrae. Dempster and colleagues[13] demonstrated that Dmab maximally preserved femoral neck cartilage remodeling while retaining modeling-based bone formation, and bone mineral density increased continuously over time. The μCT analysis of the endplate showed that after treatment with Dmab, the endplate's BMD and number of closed pores were significantly higher, while open porosity and total pore volume were significantly lower than those of the OVX + PLF group. The results of TRAP staining showed a large number of osteoclasts in cartilage endplate, bone endplate, and the junction between the endplate and vertebral body in OVX + PLF group, but the number of osteoclasts was significantly lower after Dmab treatment. This confirmed that Dmab could reduce bone conversion rate, improve the subchondral bone microstructure of endplate, and inhibit remodeling of endplate cartilage. Based on the theory that the nutrient absorption in intervertebral disc depends on endplate permeability, some studies have suggested that the increase of endplate porosity may delay the degeneration of intervertebral disc [32, 33]. However, more studies confirmed that the increase in porosity caused by endplate cartilage remodeling may be related to inflammation, excessive antigen exposure, and decreased intervertebral disc osmotic pressure, which further aggravate intervertebral disc degeneration[6, 34]. This argument has been confirmed again by the experimental results of this study. These changes may be related to the characteristics of Dmab (inhibition of osteoclast formation and activation, inhibition of osteoclast-mediated bone resorption, promotion of bone formation, and maintaining the integrity of vertebral and endplate cartilage and subchondral microstructure and function).

Intervertebral discs are a shock absorber system, and AF and NP ensure flexibility to withstand mechanical loading, which can transfer loads and dissipate energy imposed on the spine[35]. During the development of ASDD, the biomechanical changes of vertebrae hamper the dynamic balance of the spine[36]. Sakai and Grad[37] suggested that abnormal biomechanical changes of intervertebral disc can lead to local tissue injury, changed distribution of the disc's extracellular matrix and microenvironment, eventually leading to intervertebral disc degeneration. Our study revealed that, compared to the OVX + PLF group, the maximum load, yield stress, maximum stress, and elastic modulus of L6 vertebral body increased after Dmab treatment, highlighting the ability of Dmab to effectively maintain the biomechanical properties and improve the trabecular structure of the vertebral body. Intervertebral disc's matrix changes and disorders are the basic characteristics of IVDD and are also considered as potential therapeutic targets for IVDD[38, 39].

In general, NP cells produce extracellular matrix (ECM) including collagen II and proteoglycans, the main components of the gelatinous tissues of NP [20]. The gelatinous NP is essential for a functional disc, and degeneration of the NP is regarded as a crucial part of IVDD[40]. In order to evaluate the metabolic status of the intervertebral disc matrix, we detected the expression of metabolic markers by immunohistochemical staining and PCR. The results showed the expression of aggrecan was significantly higher while the expressions of ADAMT-4 and MMP-13 were significantly lower after treatment with Dmab compared to the OVX + PLF group. Safranin-O(SO) green staining showed that the structural composition of NP changed significantly in OVX + PLF group; some NP cells were replaced by chondrocyte-like cells distributed in clusters, and the matrix around NP cells had different degrees of myxoid degeneration, uneven distribution, fibrous annulus fracture, and disordered arrangement, all of which were improved in the OVX + PLF + Dmab group(Figure 11).

Conclusions

In summary, we demonstrated for the first time that ASDD induced by OVX and PLF in a rat model could be retarded by subcutaneous injections of Dmab. The protective effects of Dmab were primarily to maintain the integrity of structure and function by inhibiting vertebral osteoporosis and endplate cartilage remodeling. These findings could provide a basis for a novel therapeutic strategy for ASDD. However, our observations are still preliminary. Future studies should focus on the Dmab dose and cycle, and controlled trials should be designed to evaluate the effects of Dmab in a dose-dependent and time-dependent manner.

Abbreviations

BMD: Bone mineral density; ASDD: adjacent segmental intervertebral disc degeneration; Dmab: denosumab; μCT: microcomputed tomography; IVD: Intervertebral disc; DHI: disc height index; OVX: Ovariectomy; PLF: posterolateral lumbar fusion ; Agg: Aggrecan ;MMP-13:metalloproteinase-13 ; ADAMTS-4:a disintegrin and metalloproteinase with thrombospondin motifs 4; PO(op): Open porosity; Po.N(cl): Number of closed pores; Po.V(tot): Total volume of pore space; ROI: Region of interest; BV/TV

:bone volume fraction;Tb.N: Trabecular number; Tb.Sp: Trabecular separation; Tb.Th: Trabecular thickness; TRAP: Tartrate-resistant acid phosphatase;RT-PCR :real-time polymerase chain reaction; AF :annulus fibrosus; EP :endplates .

Declarations

Ethics approval and consent to participate

All animal experiments were approved by the Institutional Animal Care and Use Committee.

Consent for publication

Animal experiment. Not apply.

Availability of data and materials

The datasets used and/or analysed during the current study are available from the corresponding author on reasonable request.

Competing interests

The authors have no actual or potential conflict of interests including any financial, personal, or other relationships with other people or organizations that could inappropriately influence, or be perceived to influence, this paper.

Authors' contributions

Zhuang Zhou and Liu Zhang designed the study. Qi Sun, Fang Liu, Jia-Kang Fang ,Yun-Peng Hu and Qiang-Qiang-Lian keep the animal. Qi Sun analyzed the data. Fa-Ming Tian critically reviewed the data. Qi Sun drafted the manuscript. All authors contributed to interpreting the data, critically revising the manuscript, and approved the final version.

Author contributors:

Liu Zhang is the corresponding author.

Funding

This work was supported by National Natural Science Foundation of China (No. 31671235), Youth Natural Science Foundation of China (No. 81702180) and Natural Science Foundation of Hebei province (No. H2016209176), which are used for purchasing reagents and experimental animals, maintaining laboratory instruments and part of personnel costs.

Acknowledgements

No.

References

1. Ide M, Yamada K, Kaneko K, Sekiya T, Kanai K, Higashi T, et al. Combined teriparatide and denosumab therapy accelerates spinal fusion following posterior lumbar interbody fusion. Orthop Traumatol Surg Res. 2018;104:1043-48
2. Zhou Z, Tian FM, Gou Y, Wang P, Zhang H, Song HP, et al. Enhancement of Lumbar Fusion and Alleviation of Adjacent Segment Disc Degeneration by Intermittent PTH(1-34) in Ovariectomized Rats. J Bone Miner Res. 2016;31:828-38
3. Zhou Z, Tian FM, Wang P, Gou Y, Zhang H, Song HP, et al. Alendronate Prevents Intervertebral Disc Degeneration Adjacent to a Lumbar Fusion in Ovariectomized Rats. Spine (Phila Pa 1976). 2015;40:E1073-83
4. Fields AJ, Ballatori A, Liebenberg EC, Lotz JC. Contribution of the endplates to disc degeneration. Curr Mol Biol Rep. 2018;4:151-60
5. Tang Z, Hu B, Zang F, Wang J, Zhang X, Chen H. Nrf2 drives oxidative stress-induced autophagy in nucleus pulposus cells via a Keap1/Nrf2/p62 feedback loop to protect intervertebral disc from degeneration. Cell Death Dis. 2019;10:510
6. Xiao ZF, He JB, Su GY, Chen MH, Hou Y, Chen SD, et al. Osteoporosis of the vertebra and osteochondral remodeling of the endplate causes intervertebral disc degeneration in ovariectomized mice. Arthritis Res Ther. 2018;20:207
7. Ohshima H, Tsuji H, Hirano N, Ishihara H, Katoh Y, Yamada H. Water diffusion pathway, swelling pressure, and biomechanical properties of the intervertebral disc during compression load. Spine (Phila Pa 1976). 1989;14:1234-44
8. Urban JP, Holm S, Maroudas A, Nachemson A. Nutrition of the intervertebral disk. An in vivo study of solute transport. Clin Orthop Relat Res. 1977;(129):101-14
9. Maroudas A, Stockwell RA, Nachemson A, Urban J. Factors involved in the nutrition of the human lumbar intervertebral disc: cellularity and diffusion of glucose in vitro. J Anat. 1975;120:113-30
10. Holm S, Maroudas A, Urban JP, Selstam G, Nachemson A. Nutrition of the intervertebral disc: solute transport and metabolism. Connect Tissue Res. 1981;8:101-19

11. Andersen T, Christensen FB, Langdahl BL, Ernst C, Fruensgaard S, Ostergaard J, et al. Fusion mass bone quality after uninstrumented spinal fusion in older patients. Eur Spine J. 2010;19:2200-8
12. Murahashi Y, Teramoto A, Jimbo S, Okada Y, Kamiya T, Imamura R, et al. Denosumab prevents periprosthetic bone mineral density loss in the tibial metaphysis in total knee arthroplasty. Knee. 2020, 10.1016/j.knee.2019.12.010
13. Dempster DW, Chines A, Bostrom MP, Nieves JW, Zhou H, Chen L, et al. Modeling-Based Bone Formation in the Human Femoral Neck in Subjects Treated With Denosumab. J Bone Miner Res. 2020, 10.1002/jbmr.4006
14. O'Loughlin PF, Cunningham ME, Bukata SV, Tomin E, Poynton AR, Doty SB, et al. Parathyroid hormone (1-34) augments spinal fusion, fusion mass volume, and fusion mass quality in a rabbit spinal fusion model. Spine (Phila Pa 1976). 2009;34:121-30
15. Abe Y, Takahata M, Ito M, Irie K, Abumi K, Minami A. Enhancement of graft bone healing by intermittent administration of human parathyroid hormone (1-34) in a rat spinal arthrodesis model. Bone. 2007;41:775-85
16. DePalma AF, Rothman RH. The nature of pseudarthrosis. Clin Orthop Relat Res. 1968;59:113-8
17. Lu DS, Shono Y, Oda I, Abumi K, Kaneda K. Effects of chondroitinase ABC and chymopapain on spinal motion segment biomechanics. An in vivo biomechanical, radiologic, and histologic canine study. Spine (Phila Pa 1976). 1997;22:1828-34; discussion 34-5
18. Masuda K, Aota Y, Muehleman C, Imai Y, Okuma M, Thonar EJ, et al. A novel rabbit model of mild, reproducible disc degeneration by an anulus needle puncture: correlation between the degree of disc injury and radiological and histological appearances of disc degeneration. Spine (Phila Pa 1976). 2005;30:5-14
19. Livak KJ, Schmittgen TD. Analysis of relative gene expression data using real-time quantitative PCR and the 2(-Delta Delta C(T)) Method. Methods. 2001;25:402-8
20. Wu X, Liu Y, Guo X, Zhou W, Wang L, Shi J, et al. Prolactin inhibits the progression of intervertebral disc degeneration through inactivation of the NF-kappaB pathway in rats. Cell Death Dis. 2018;9:98
21. Lawrence BD, Wang J, Arnold PM, Hermsmeyer J, Norvell DC, Brodke DS. Predicting the risk of adjacent segment pathology after lumbar fusion: a systematic review. Spine (Phila Pa 1976). 2012;37:S123-32
22. Park SB, Chung CK. Strategies of spinal fusion on osteoporotic spine. J Korean Neurosurg Soc. 2011;49:317-22
23. Liu CC, Tian FM, Zhou Z, Wang P, Gou Y, Zhang H, et al. Protective effect of calcitonin on lumbar fusion-induced adjacent-segment disc degeneration in ovariectomized rat. BMC Musculoskelet Disord. 2015;16:342
24. Crock HV, Goldwasser M. Anatomic studies of the circulation in the region of the vertebral end-plate in adult Greyhound dogs. Spine (Phila Pa 1976). 1984;9:702-6
25. Bellido M, Lugo L, Roman-Blas JA, Castaneda S, Caeiro JR, Dapia S, et al. Subchondral bone microstructural damage by increased remodelling aggravates experimental osteoarthritis preceded

by osteoporosis. Arthritis Res Ther. 2010;12:R152

26. Shapiro IM, Vresilovic EJ, Risbud MV. Is the spinal motion segment a diarthrodial polyaxial joint: what a nice nucleus like you doing in a joint like this? Bone. 2012;50:771-6
27. Yishake M, Yasen M, Jiang L, Liu W, Xing R, Chen Q, et al. Effects of combined teriparatide and zoledronic acid on posterior lumbar vertebral fusion in an aged ovariectomized rat model of osteopenia. J Orthop Res. 2018;36:937-44
28. Etebar S, Cahill DW. Risk factors for adjacent-segment failure following lumbar fixation with rigid instrumentation for degenerative instability. J Neurosurg. 1999;90(2 Suppl):163-9
29. Zhu J, Tang H, Zhang Z, Zhang Y, Qiu C, Zhang L, et al. Kaempferol slows intervertebral disc degeneration by modifying LPS-induced osteogenesis/adipogenesis imbalance and inflammation response in BMSCs. Int Immunopharmacol. 2017;43:236-42
30. Tsai JN, Uihlein AV, Lee H, Kumbhani R, Siwila-Sackman E, McKay EA, et al. Teriparatide and denosumab, alone or combined, in women with postmenopausal osteoporosis: the DATA study randomised trial. Lancet. 2013;382:50-6
31. Cummings SR, San Martin J, McClung MR, Siris ES, Eastell R, Reid IR, et al. Denosumab for prevention of fractures in postmenopausal women with osteoporosis. N Engl J Med. 2009;361:756-65
32. Ding Y, Jiang J, Zhou J, Wu X, Huang Z, Chen J, et al. The effects of osteoporosis and disc degeneration on vertebral cartilage endplate lesions in rats. Eur Spine J. 2014;23:1848-55
33. Tomaszewski KA, Adamek D, Konopka T, Tomaszewska R, Walocha JA. Endplate calcification and cervical intervertebral disc degeneration: the role of endplate marrow contact channel occlusion. Folia Morphol (Warsz). 2015;74:84-92
34. Xiao ZF, Su GY, Hou Y, Chen SD, Zhao BD, He JB, et al. Mechanics and Biology Interact in Intervertebral Disc Degeneration: A Novel Composite Mouse Model. Calcif Tissue Int. 2020;106:401-14
35. Iatridis JC. Tissue engineering: Function follows form. Nat Mater. 2009;8:923-4
36. Yasen M, Li X, Jiang L, Yuan W, Che W, Dong J. Effect of zoledronic acid on spinal fusion outcomes in an ovariectomized rat model of osteoporosis. J Orthop Res. 2015;33:1297-304
37. Stokes IA, Iatridis JC. Mechanical conditions that accelerate intervertebral disc degeneration: overload versus immobilization. Spine (Phila Pa 1976). 2004;29:2724-32
38. Silagi ES, Shapiro IM, Risbud MV. Glycosaminoglycan synthesis in the nucleus pulposus: Dysregulation and the pathogenesis of disc degeneration. Matrix Biol. 2018;71-72:368-79
39. Bedore J, Leask A, Seguin CA. Targeting the extracellular matrix: matricellular proteins regulate cell-extracellular matrix communication within distinct niches of the intervertebral disc. Matrix Biol. 2014;37:124-30
40. Wang K, Chen T, Ying X, Zhang Z, Shao Z, Lin J, et al. Ligustilide alleviated IL-1beta induced apoptosis and extracellular matrix degradation of nucleus pulposus cells and attenuates

intervertebral disc degeneration in vivo. Int Immunopharmacol. 2019;69:398-407

Figures

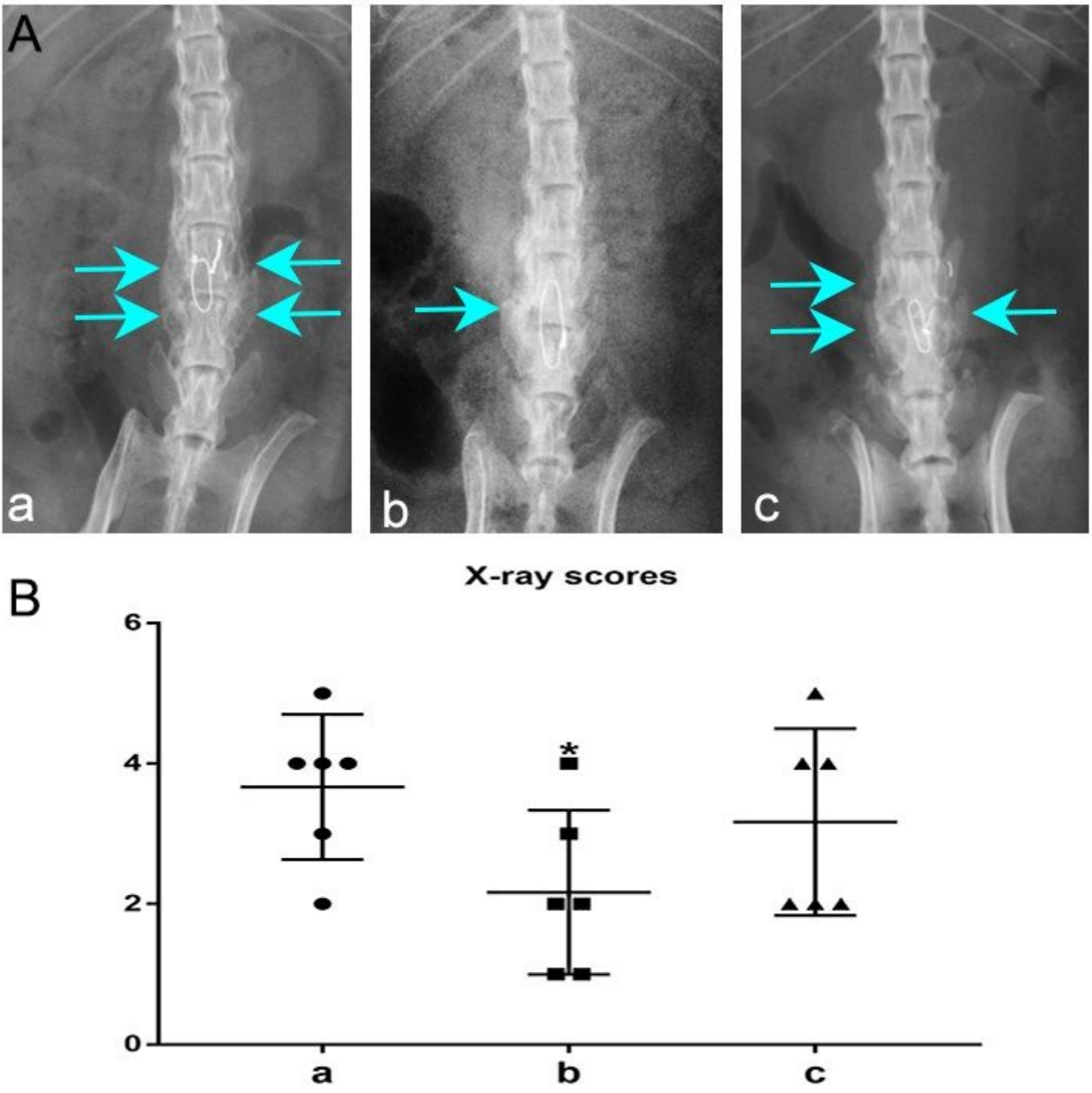

Figure 1

Radiographic evaluation of lumbar fusion at 4 weeks post-PLF. (A) Representative radiographic images of three groups. PLF of the L4–L5 segment was performed using an intertransverse process fusion with

an autologous iliac bone graft and spinous-process wire fixation. Compared to the OVX+PLF group, OVX+PLF+Dmab group showed a higher radiographic density with more new bone formation (thin arrow). (B) X-ray scores of lumbar fusion. Note: *P<0.05 vs. the Sham group. a: PLF, b: OVX+PLF group, c: OVX+PLF+Dmab group

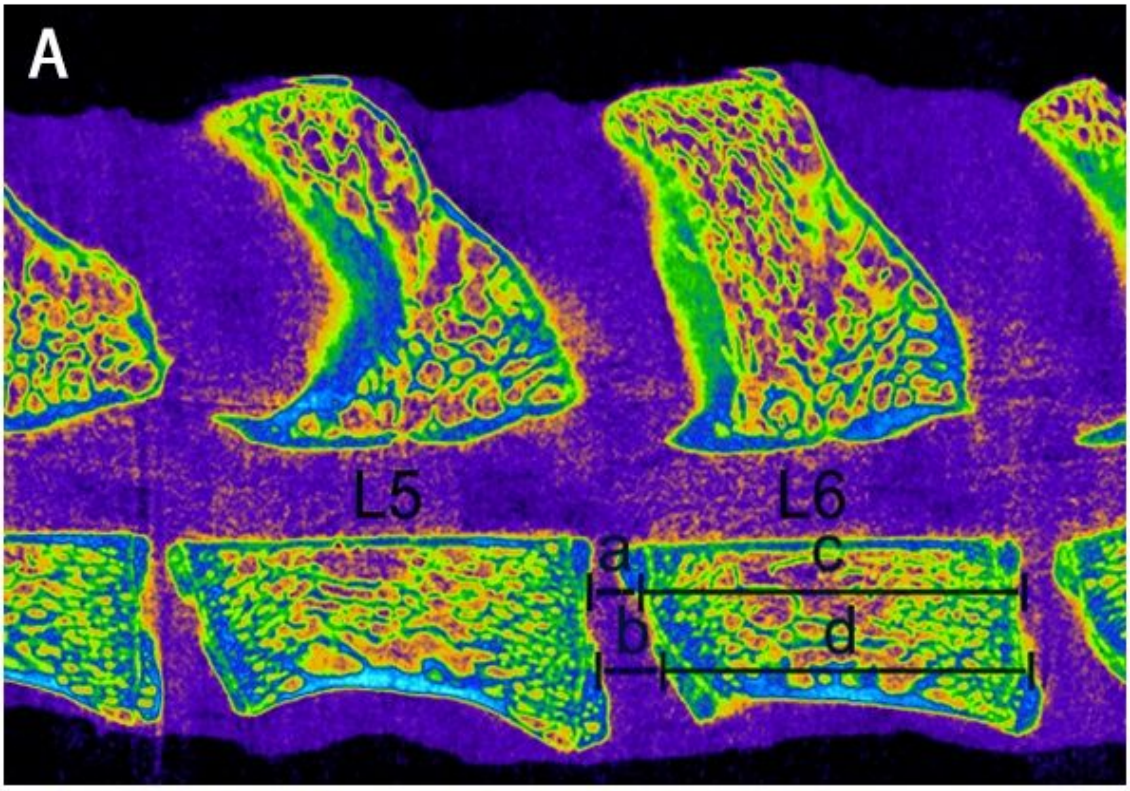

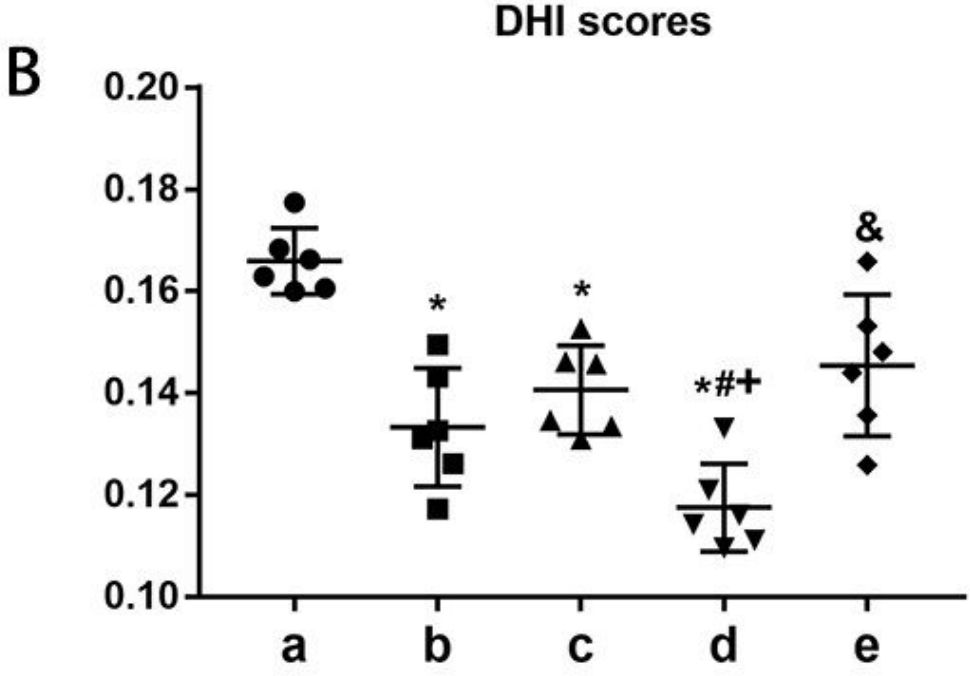

Figure 2

Representative micro-CT image of the lumbar spine used to quantify the DHI between the L5 and L6 vertebrae, calculated based on measurements of the adjacent L6 vertebra (A). DHI was calculated using the following equation: DHI= (a+b)/(c+d). The changes of DHI in all groups (B). Note: *P < 0.05 vs. Sham group; #P < 0.05 vs. OVX group;+P < 0.05 vs. PLF group; &P < 0.05 vs. OVX+PLF group. a: Sham group, b: OVX group, c: PLF group, d: OVX+PLF group, e: OVX+PLF+Dmab group

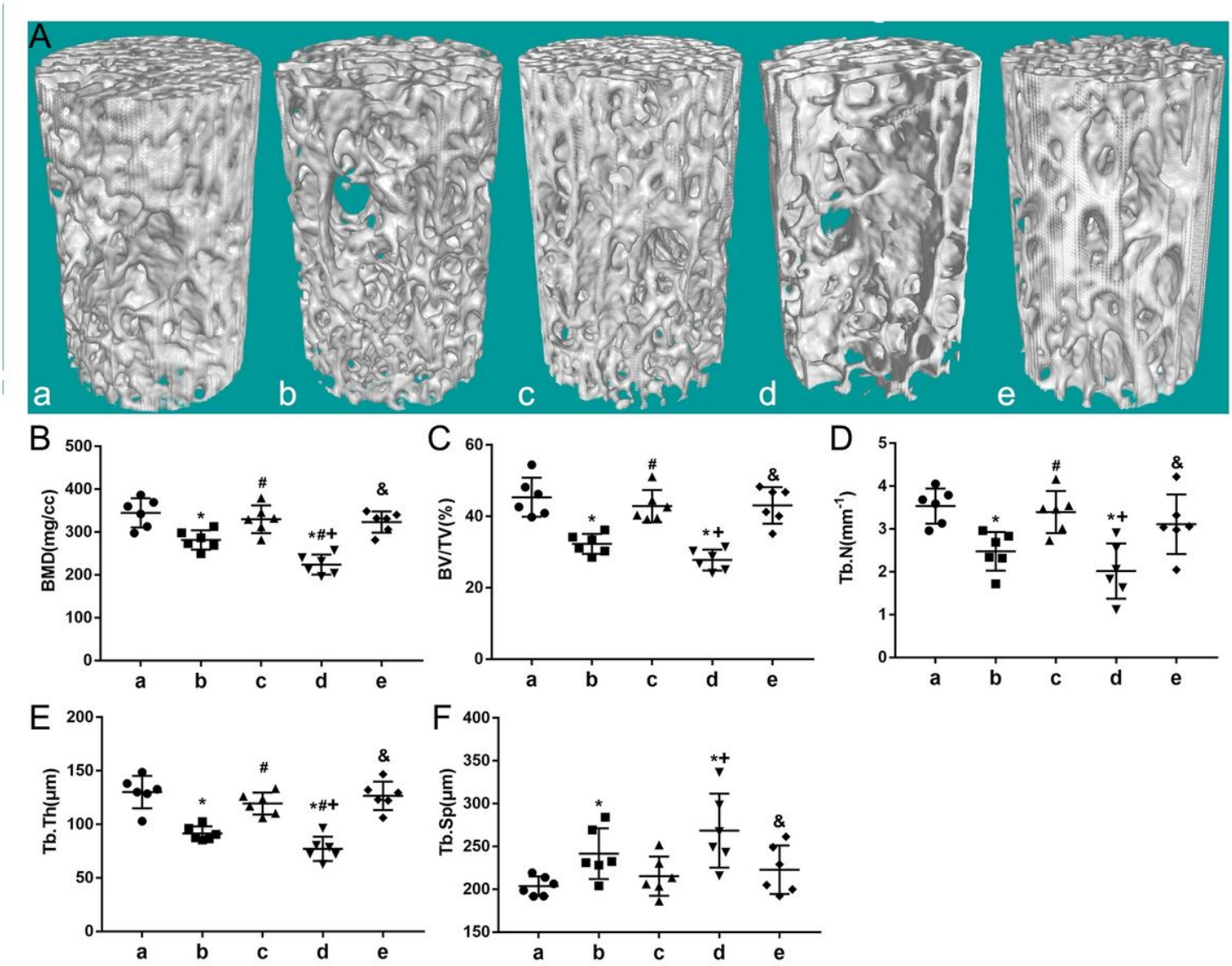

Figure 3

Representative micro-CT image of L6 vertebra (A). Compared to the Sham group, the trabeculae were sparser and the width of the canal between trabeculae was higher in the OVX and OVX+PLF groups, and even a large area of bone trabeculae was missing in the OVX+PLF group. The parameters of L6 trabecular bone (B-F). The results of L6 vertebral BMD, bone volume (BV)/total volume (TV), trabecular number (Tb.N; mm-1), trabecular thickness (Tb.Th; μm), and trabecular separation (Tb.Sp; μm) in different groups. Note: *P < 0.05 vs. Sham group; #P < 0.05 vs. OVX group; +P < 0.05 vs. PLF group; &P <

0.05 vs. OVX+PLF group. a: Sham group, b: OVX group, c: PLF group, d: OVX+PLF group, e: OVX+PLF+Dmab group

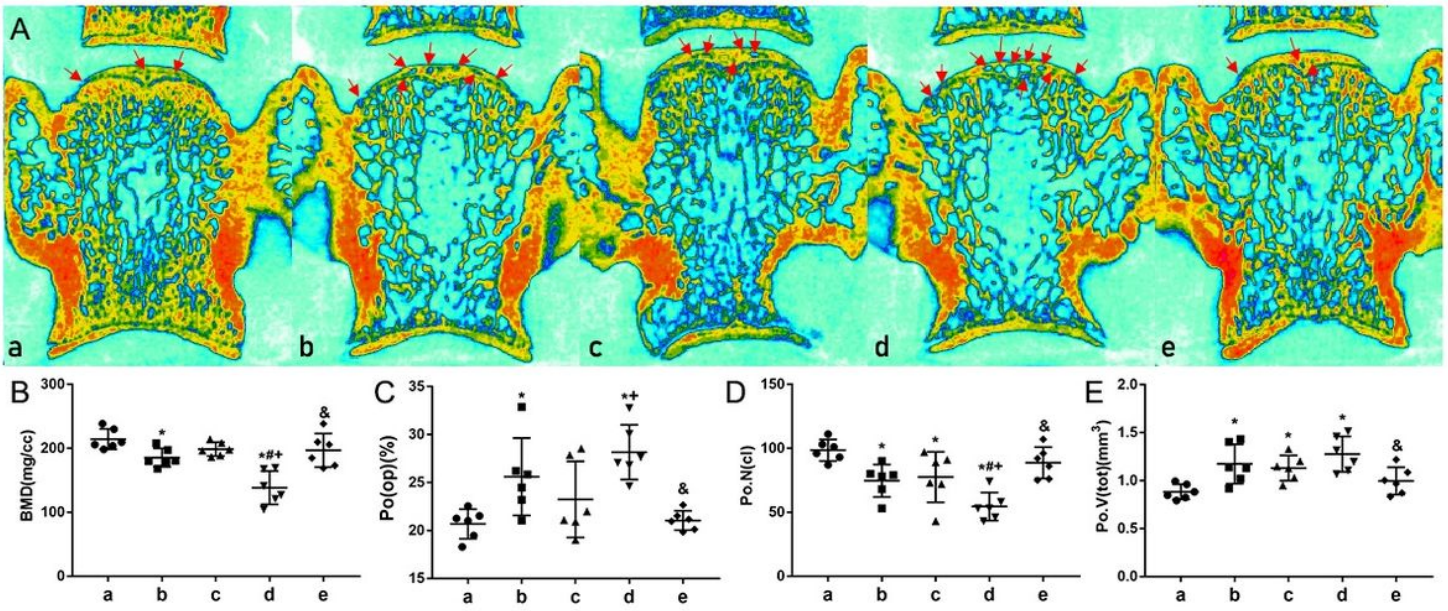

Figure 4

Changes in microarchitecture and porosity of L5/6 caudal endplate quantified by μCT analysis. Representative coronal images and parameters of caudal endplate in all groups (A). More cavities in OVX and OVX+PLF rats (red arrow) indicate osteochondral remodeling of the endplate. (B-D) Compared to the Sham group, markedly lower number of closed pores (Po.N(cl)), higher open porosity (Po(op)), and total pore volume (Po.V(tot)) occurred in the OVX and OVX+PLF groups. OVX+PLF+Dmab group showed a significantly higher number of closed pores and lower open porosity (Po(op)) and total volume of pore space (Po.V(tot)) compared to the OVX+PLF group. Note: *P < 0.05 vs. Sham group; #P < 0.05 vs. OVX group; +P < 0.05 vs. PLF group; &P < 0.05 vs. OVX+PLF group. a: Sham group, b: OVX group, c: PLF group, d: OVX+PLF group, e: OVX+PLF+Dmab group

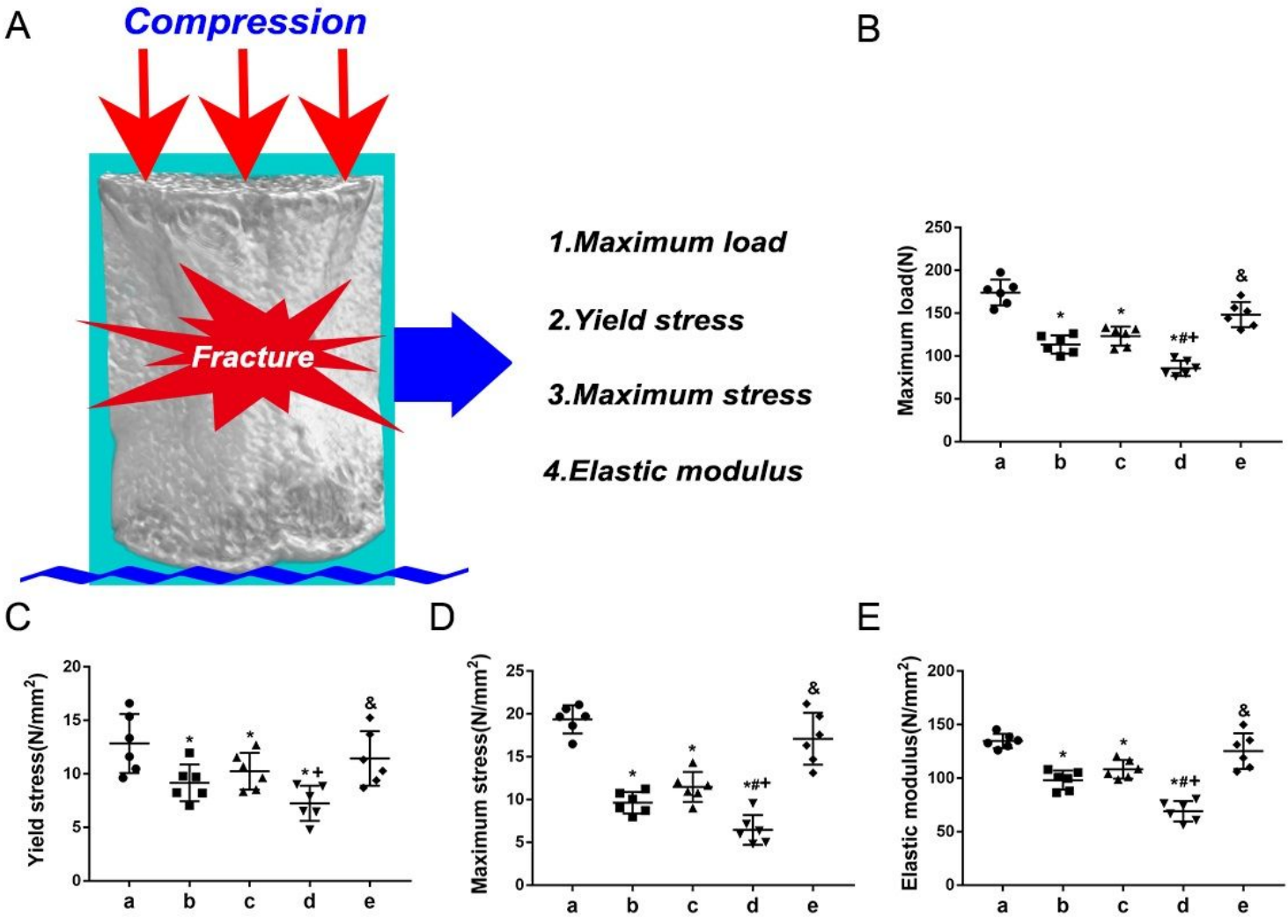

Figure 5

Diagram of L6 vertebral body compression experiment (A) and the results of mechanical properties in all groups (B-E). Compared to the Sham group, markedly lower maximum load, yield stress, maximum stress, and elastic modulus values were found in the OVX and OVX+PLF groups. Dmab treatment increased the above indices significantly compared to the OVX+PLF group. Note: *P < 0.05 vs. Sham group; #P < 0.05 vs. OVX group; +P < 0.05 vs. PLF group; &P < 0.05 vs. OVX+PLF group. a: Sham group, b: OVX group, c: PLF group, d: OVX+PLF group, e: OVX+PLF+Dmab group.

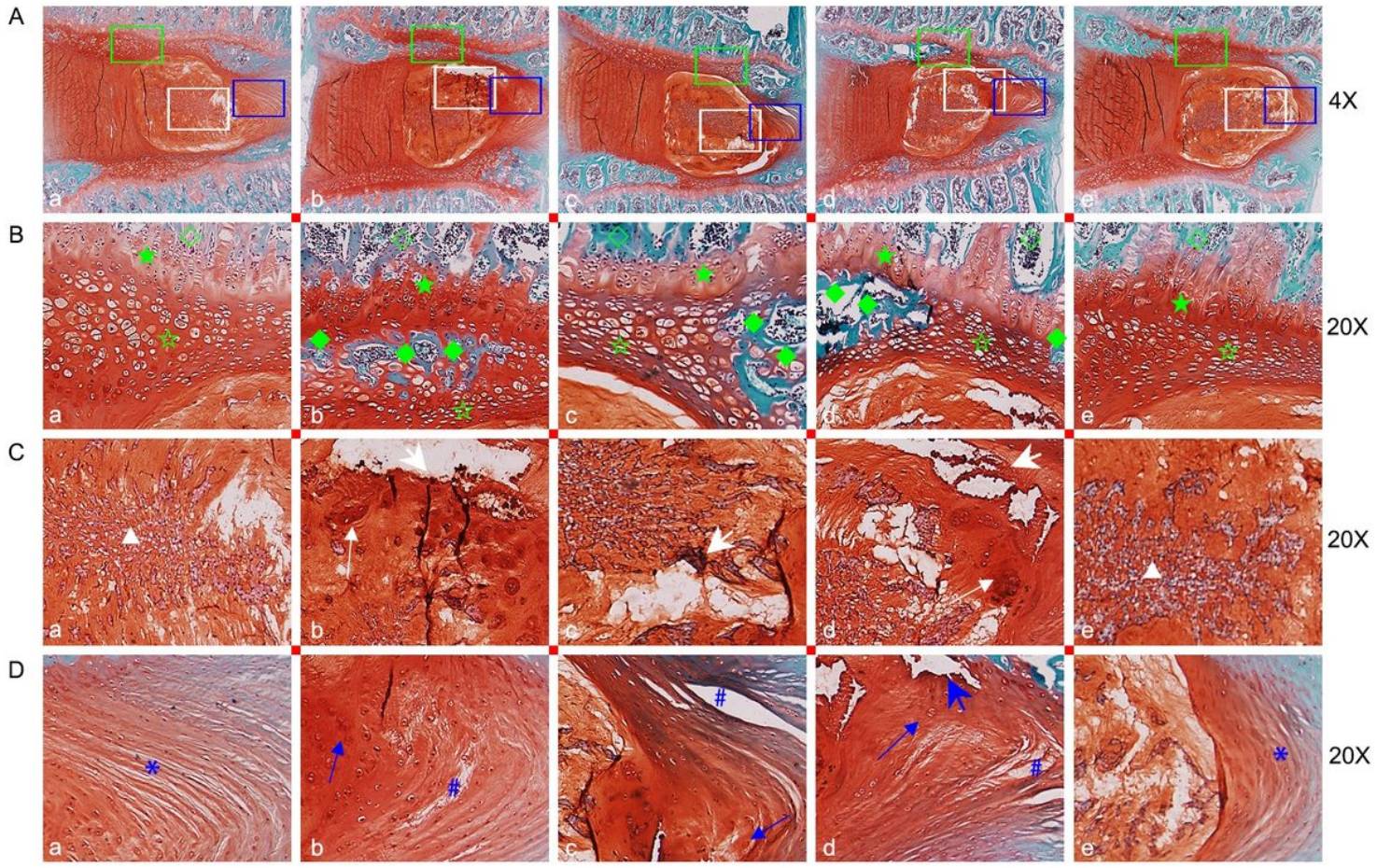

Figure 6

Histological illustration of the L5–L6 segments of the lumbar spine in different groups. (A) Safranin O and fast green staining of the L5–L6 (×4). (B) Safranin O and fast green staining of cartilage endplate. Green hollow pentagram indicates cartilage endplate cells, and green solid quadrilateral indicates new bony tissue (×20). (C) The degenerative changes in the nucleus pulposus visualized with safranin O and fast green staining. A white triangle indicates notochord cells, white thin arrow indicates chondrocyte-like cells, and white large arrow indicates mucoid degeneration (×20). (D) Safranin O and fast green staining of annulus fibrosus (blue asterisk indicates regular annulus fibrosus, blue pound sign indicates cleft/crack, blue thin arrow indicates chondrocyte-like cells, and blue large arrow indicates mucoid degeneration in the annulus fibrosus) (×20). Note: *P < 0.05 vs. Sham group; #P < 0.05 vs. OVX group; +P < 0.05 vs. PLF group; &P < 0.05 vs. OVX+PLF group. a: Sham group, b: OVX group, c: PLF group, d: OVX+PLF group, e: OVX+PLF+Dmab group. □, vertebral epiphysis; □, cartilage endplate; □, vertebral physis; □, bony tissue.

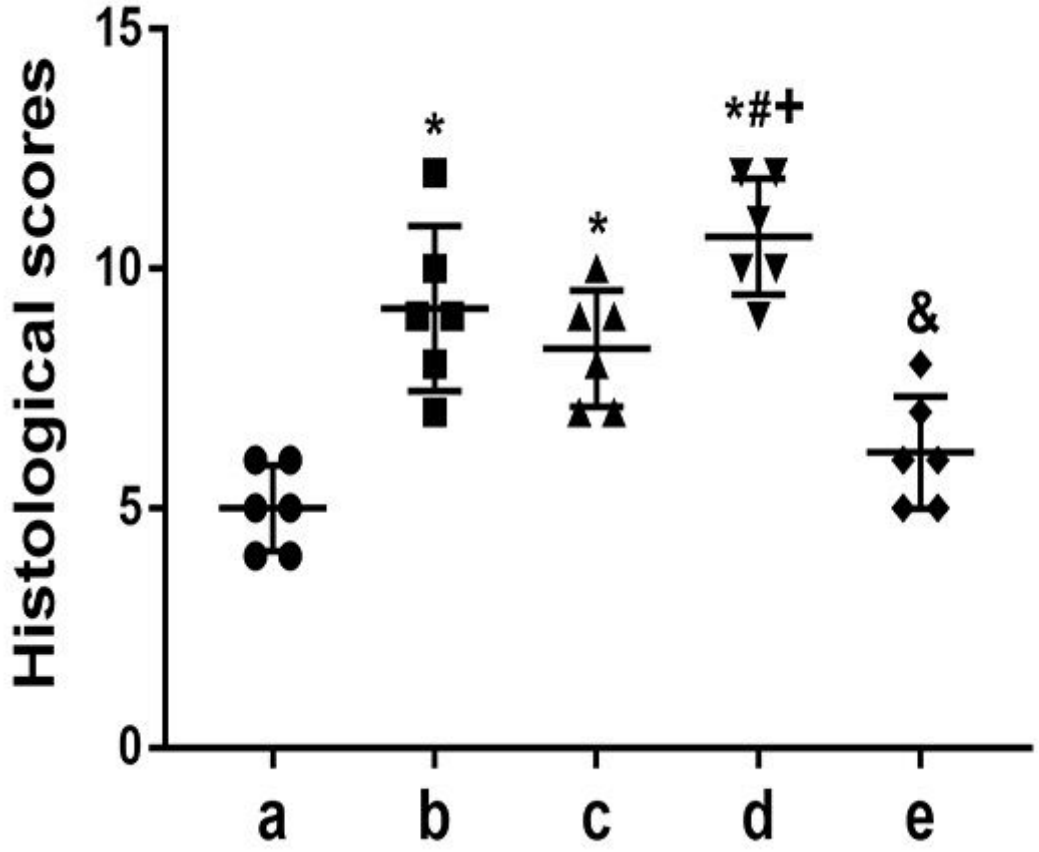

Figure 7

Histological scores of the L5–L6 intervertebral disc in different groups. Note: *P < 0.05 vs. Sham group; #P < 0.05 vs. OVX group; +P < 0.05 vs. PLF group; &P < 0.05 vs. OVX+PLF group. a: Sham group, b: OVX group, c: PLF group, d: OVX+PLF group, e: OVX+PLF+Dmab group

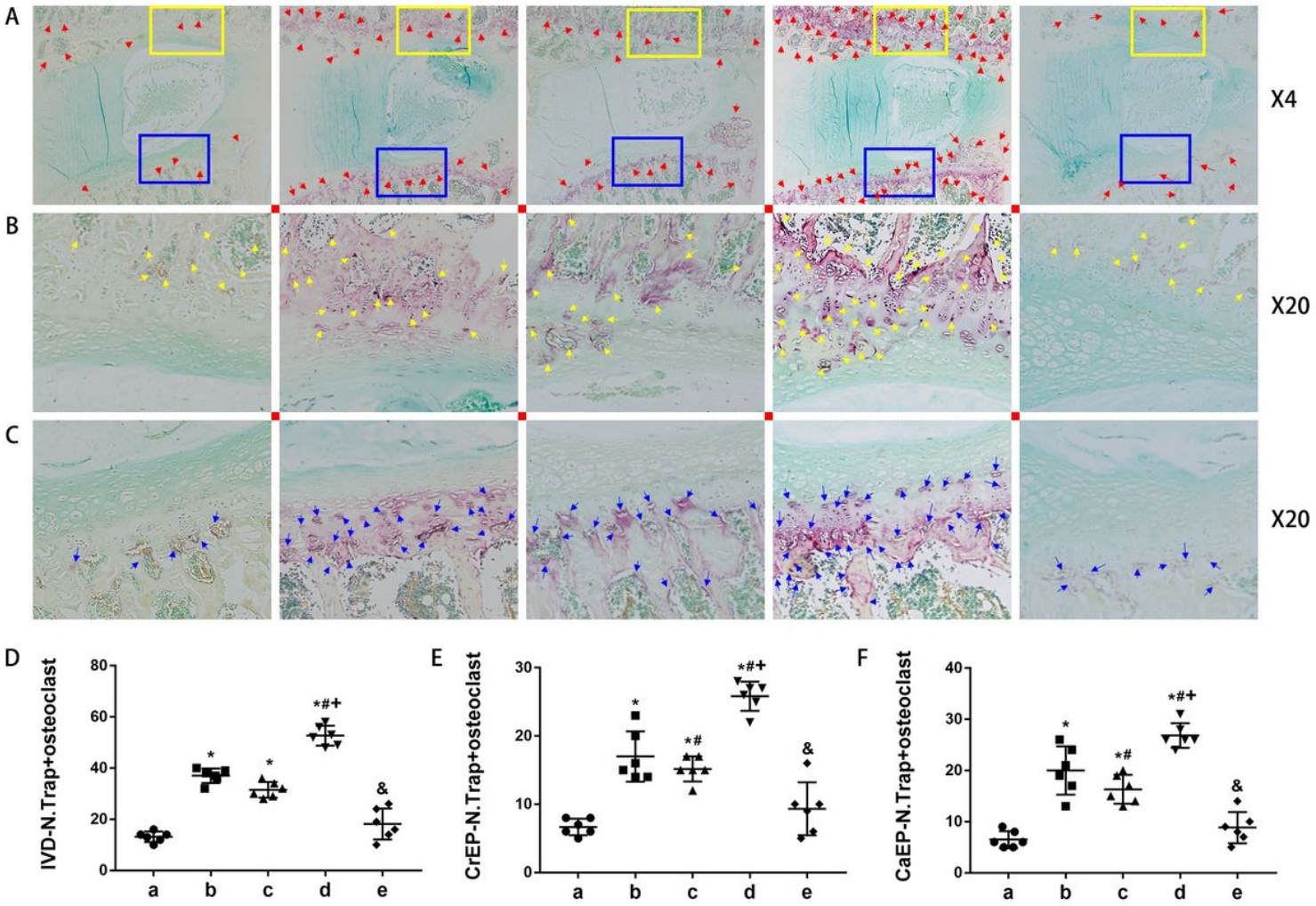

Figure 8

Tartrate acid phosphatase (TRAP) staining of L5/6. The osteoclasts were obtained by counting the number of TRAP-positive cells (N. Trap+). (A) A few TRAP-positive cells (purple; red arrows) were distributed on the surface of the trabeculae of the subchondral bone and were rarely detected in the endplate of Sham and OVX+PLF groups (×4). However, TRAP-positive cells (purple; red arrows) were significantly more frequent in the subchondral bone and the endplate of OVX+PLF group, suggesting a reduced osteoclast activity after Dmab treatment. (B) TRAP staining of CrEP (purple; yellow arrows) (×20). (C) TRAP staining of CaEP (purple; blue arrows) (×20), Note: *P < 0.05 vs. Sham group; #P < 0.05 vs. OVX group; +P < 0.05 vs. PLF group; &P < 0.05 vs. OVX+PLF group. a: Sham group, b: OVX group, c: PLF group, d: OVX+PLF group, e: OVX+PLF+Dmab group. IVD intervertebral disc, CrEP cranial endplate, CaEP caudal endplate

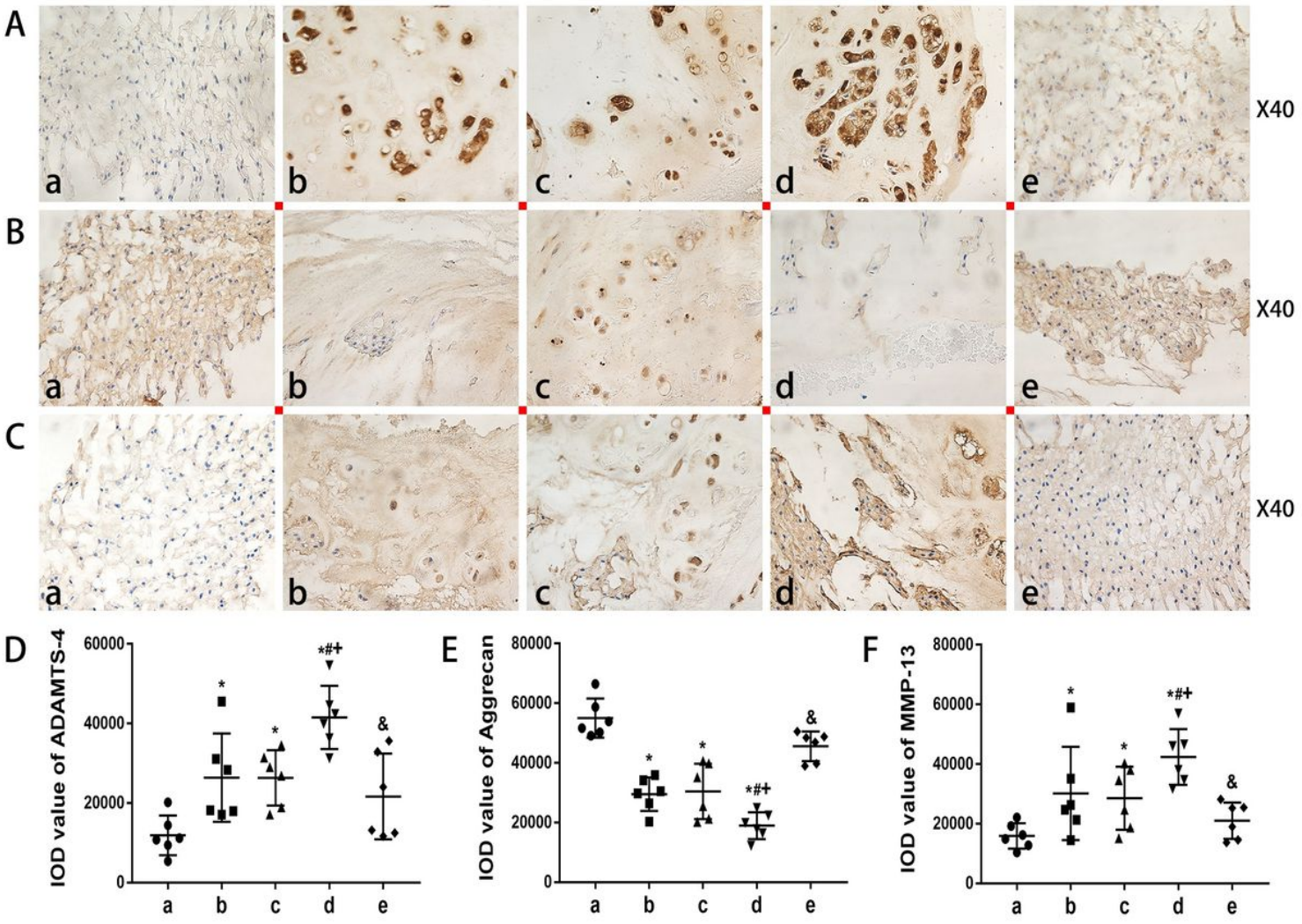

Figure 9

Immunohistochemistry assay for (A) ADAMTS-4, (B) aggrecan, and (C) MMP-13 in the nucleus pulposus in different groups (×40). Immunohistological analysis showed that the protein expression of aggrecan in the OVX+PLF+Dmab group was higher than that in the OVX+PLF group. MMP-13 and ADAMTS-4-positive staining in the nucleus pulpous was weaker in the OVX+PLF+Dmab group compared to the OVX+PLF group. Note: *P < 0.05 vs. Sham group; #P < 0.05 vs. OVX group; +P < 0.05 vs. PLF group; &P < 0.05 vs. OVX+PLF group. a: Sham group, b: OVX group, c: PLF group, d: OVX+PLF group, e: OVX+PLF+Dmab group

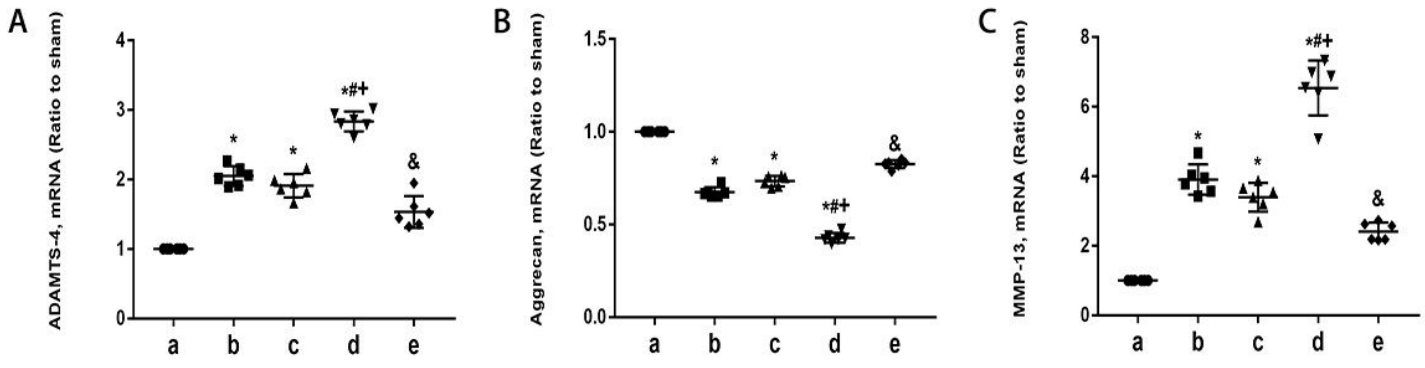

Figure 10

mRNA expression of ADAMTS-4, aggrecan, and MMP-13 in different groups. Note: *P < 0.05 vs. Sham group; #P < 0.05 vs. OVX group; +P < 0.05 vs. PLF group; &P < 0.05 vs. OVX+PLF group.

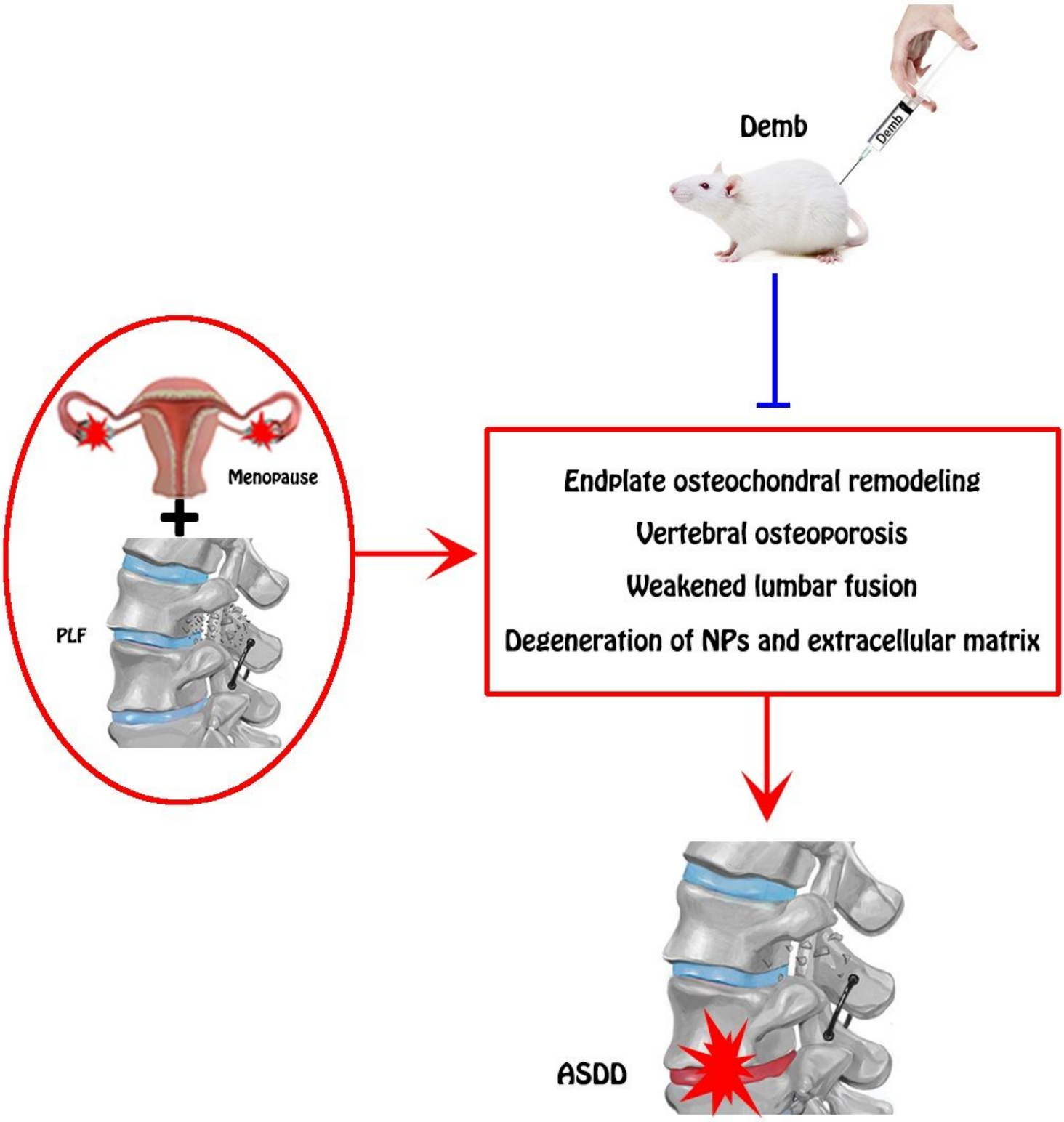

Figure 11

Potential mechanism of Dmab in the treatment of ASDD in rats. Dmab enhances lumbar fusion and alleviates ASDD in NP cells via suppressing endplate osteochondral remodeling, vertebral osteoporosis, and ECM degradation.